Calibration Transfer from Micro NIR Spectrometer to Hyperspectral Imaging: a Case Study on Predicting Soluble Solids Content of Bananito Fruit (Musa acuminata)

Article *in* Food Analytical Methods · April 2018

DOI: 10.1007/s12161-017-1055-3

CITATIONS
35

READS
1,524

7 authors, including:

Yuan-Yuan Pu
TEAGASC - The Agriculture and Food Development Authority
21 PUBLICATIONS **1,033** CITATIONS
SEE PROFILE

Da-Wen Sun
University College Dublin
1,005 PUBLICATIONS **64,186** CITATIONS
SEE PROFILE

Cecilia Riccioli
PerkinElmer
33 PUBLICATIONS **623** CITATIONS
SEE PROFILE

Marina Buccheri
Council for Agricultural Research and Agricultural Economy Analysis
54 PUBLICATIONS **589** CITATIONS
SEE PROFILE

Food Anal. Methods
https://doi.org/10.1007/s12161-017-1055-3

Calibration Transfer from Micro NIR Spectrometer to Hyperspectral Imaging: a Case Study on Predicting Soluble Solids Content of Bananito Fruit (*Musa acuminata*)

Yuan-Yuan Pu[1] · **Da-Wen Sun**[1] · **Cecilia Riccioli**[2] · **Marina Buccheri**[3] · **Maurizio Grassi**[3] · **Tiziana M. P. Cattaneo**[3] · **Aoife Gowen**[1]

Received: 19 July 2017 / Accepted: 5 October 2017

Abstract Calibration transfer from a handheld micro NIR spectrometer (NIR-point, 939–1602 nm, 6.2 nm) to a desktop hyperspectral imaging (NIR-HSI) for predicting soluble solids content (SSC) of bananito flesh was investigated in the study. Different spectral pre-processing and standardization methods were employed for correcting spectra so as to minimise spectral differences between NIR-point and NIR-HSI. Results show that application of standard normal variate (SNV) reduced spectral differences from 31.49 to 8.96%. The best standardization method was developed based on piecewise direct standardization (PDS) algorithm using ten transfer samples. The developed PLS model yielded a high prediction performance (R^2_p = 0.922 and RMSEP = 1.451%) for predicting SSC of validation samples using the NIR-point spectra. After SNV and standardization, the model was successfully transferred to NIR-HSI data, giving a comparable prediction accuracy of R^2_p = 0.925 and RMSEP = 1.592%. The results illustrated the potential of transferring calibration models from a simple and easy-available micro NIR spectrometer to a more expensive and sophisticated hyperspectral imaging system, when the spatial distribution of quality information is required.

Keywords Calibration transfer · Standardization · Soluble solids content · Near-infrared · Spectrometer · Hyperspectral imaging

Introduction

Quality plays a critical role for the food industry. The industry not only requires techniques such as cooling (McDonald et al. 2000; Sun and Brosnan 1999; Zheng and Sun 2004; Sun and Zheng 2006; McDonald et al. 2001; Wang and Sun 2004; Sun 1997), freezing (Kiani et al. 2011; Ma et al. 2015; Xie et al. 2015; Cheng et al. 2016a; Pu et al. 2015a; Cheng et al. 2017; Xie et al. 2016) and drying (Delgado and Sun 2002; Sun 1999; Yang et al. 2017; Pu and Sun 2016; Qu et al. 2017; Ma et al. 2017; Pu et al. 2017) to maintain food quality, but it also needs techniques for quality assessment. Therefore, many techniques such as spectroscopy (Nicolaï et al. 2007), computer vision (Jackman et al. 2009; Du and Sun 2005; Sun and Brosnan 2003; Jackman et al. 2011; Xu et al. 2017) and spectral imaging (Feng et al. 2013a, b; Kamruzzaman et al. 2013; Wu and Sun 2013; ElMasry et al. 2013; Cheng et al. 2015a, b; Xiong et al. 2015; Pu et al. 2015b; Ma et al. 2016; Cheng et al. 2016b; Cheng and Sun 2017; Li et al. 2017) have been investigated to provide alternative quality detection tools for the industry. Among them is near-infrared (NIR) spectrometry has been developed as one of the most important process analytical tools (PAT) for rapid and non-destructive quality assessment in a variety of areas (Luypaert et al. 2007, Pojić and Mastilović 2013, Woodcock et al. 2008, Tsuchikawa 2007). The use of chemometric techniques is powerful in revealing qualitative and quantitative information concealed in the NIR spectra. Handheld Fourier transform NIR instruments are also popular for on-site measurement of fruit qualities to provide a quick, flexible, and non-destructive analysis (Schmutzler and Huck 2016, Ignat et al. 2014, Antonucci et al. 2011). In industrial applications, several

✉ Da-Wen Sun
dawen.sun@ucd.ie; http://www.ucd.ie/refrig; http://www.ucd.ie/sun

[1] School of Biosystems and Food Engineering, University College Dublin, National University of Ireland, Dublin 4, Ireland

[2] Faculty of Agriculture and Forestry Engineering, Department of Animal Production, University of Cordoba, Campus Rabanales, Ctra.Nacional IV – Km 396, 14071 Cordoba, Spain

[3] Council for Agricultural Research and Economics (CREA-IT), via Venezian 26, 20133 Milan, Italy

Published online: 30 October 2017

NIR instruments may be used at the same time to collect spectra of samples distributed along the manufacturing chain. Variations in instrument components (optics or new replacements) and detecting environment (temperature and humidity) (Huang et al. 2010) result in spectral differences of the same samples. As a result, a robust calibration model developed on one instrument might not work well on the spectra acquired from another instrument of the same mode. To develop a calibration model for each individual instrument is not an economic practice as it brings extra time and cost for sampling and calibrating. To address this issue, the study of spectral standardization and calibration transfer is needed.

Calibration transfer refers to a standardization procedure that enables calibration models developed on one instrument (commonly known as 'master' instrument) to be further used on another instrument or more ('slaves'). As summarised in the review of Fearn (2001) and Feudale et al. (2002), calibration models could be transferred by either adjusting the calibration model by slope and bias correction or correcting the slave spectra to make it look as if they were derived from the master instrument. The second strategy is frequently used. There are two main approaches for spectra correction. One is to pre-process spectra before model transfer, so as to reduce or even remove undesired spectral responses such as scattering effects, waveband shift, baseline, or offsets that could affect the model performance. A number of techniques for pre-processing of spectroscopic data were introduced by Rinnan et al. (2009) and Huang et al. (2010), with details of principles and application given. Briefly, techniques like standard normal variate (SNV), multiplicative scatter correction (MSC), and normalisation attempted to reduce spectral scattering. Spectral derivatives including Norris-Williams derivation and Savitzky-Golay polynomial derivation of different orders help to remove baseline drift, distinguish overlap peaks, or extract important signals. The other approach is to develop a standardization model within master and slave instruments based on a small amount of transfer samples. A variety of standardization algorithms have been proposed for instrument standardization and multivariate model transfer. The most widely used methods are direct standardization (DS) (Wang et al. 1991), piecewise direct standardization (PDS) (Bouveresse et al. 1996) or double window piecewise direct standardization (DWPDS) (Wise et al. 2006), and orthogonal signal correction (OSC) (Sjöblom et al. 1998). Several improved or new methods were also reported in the literature, for example Rank-Kennard-Stone-PDS (Liang et al. 2016), the boxcar signal transfer (BST) (Oliveri et al. 2013), spectral difference at each wavelength (SDW) (Pierna et al. 2010), and alternating trilinear decomposition (ATLD) (Liu et al. 2014), with satisfactory transfer results obtained.

Practical applications of instrument standardization and calibration transfer in NIR spectroscopy started from the investigation of model transfer between spectrometers of the same mode (Shenk et al. 1985). Temperature compensation was also considered to reduce spectral variations caused by temperature fluctuations in the working environment (Wang and Kowalski 1993). Recent development focused on transferring multivariate calibration models among multiple spectrometers (Ge et al. 2011, Liu et al. 2014), among instruments from different manufacturers (Pereira et al. 2008, Woody et al. 2004) and located in different countries (Grelet et al. 2015). The success of transferring calibration models from a dispersive NIR instrument to a handheld spectrometer for predicting fat, fibre, protein, and starch of feed products was reported by Pierna et al. (2010), which demonstrated the feasibility of transferring calibrations from laboratory to on-site instruments (Soldado et al. 2013, Zamora-Rojas et al. 2012). A novel application of calibration transfer in pharmaceutical formulations was proposed by Pereira et al. (2016), who applied the DWPDS standardization technique to spectra of samples in powder mixtures and intact tablets. The partial least square (PLS) model developed on powder mixtures was successfully transferred to intact tablets for nevirapine prediction. This study explored the potential of using calibration transfer between samples spectra of different physical forms, suggesting the use of one calibration model over a processing chain particularly in pharmaceutical industry to reduce modelling cost. This application could be extended to other matrices in different physical conditions, for example tobacco powders and flakes (Qin and Gong 2016).

Hyperspectral imaging (HSI) technique (ElMasry and Sun 2010, Ravikanth et al. 2017, Lorente et al. 2012) is an advanced extension of the probe-based spectrometers. It can be seen as a system that integrates tens of thousands of mini-spectrometers located in each point of the scanned sample (Liu et al. 2007). The combined device of a camera and a spectrograph assembles all spectra from every single point of the sample to construct a three-dimensional database, which allows spectral and spatial information of products to be accessed at the same time. Additionally, image acquisition can be accomplished by line-scanned or area-scanned, providing a fast and chemical-free data collection procedure to most efficiently achieve real-time analysis. These outstanding features in HSI significantly broaden its applications in the last 2 decades, particularly in agri-food area (Gowen et al. 2007, Zhu et al. 2013, Liu et al. 2014) and pharmaceutical industry (Gendrin et al. 2008) where samples with an uneven distribution property (chemical components, defects, or contaminants) could be visualised from the final prediction maps. Nevertheless, HSI should be used properly only when it is necessarily needed (Amigo et al. 2015), i.e. where there is a spatial variation on the sample, as in some cases the use of spectrometers is sufficient to address the problem. Despite all those figures of merit, HSI has its disadvantages. The costs of the whole system and attached software are expensive. In addition, a high-performance computer with a large storage space and computing capability is essential for processing such a huge amount of data.

From an industrial application point of view, when a new hyperspectral imaging system is introduced to the industry, it is more practical and cost-effective to transfer current available calibration models to the hyperspectral imaging system using a small number of transfer samples, rather than re-

calibrating the whole models based on new samples and new instruments. As mentioned above, transferring calibration models between different NIR spectrometers has been extensively reported. However, to the best of our knowledge, limited information is currently available on the transfer of calibration models developed on point-measured spectrometers to space-measured hyperspectral imaging data.

This study investigated the potential of transferring a multivariate calibration model from a handheld micro spectrometer to a desktop hyperspectral imaging system, on a case of predicting soluble solids content of bananito flesh. Bananito fruit [*Musa acuminata* (AA)] is a small banana type that provides a sweet and creamy flavour. The soluble solids in bananito flesh include all compounds that are soluble in water, i.e. sugars, organic acids, amino acids, phenolic compounds, vitamins, and some soluble pectin. The soluble solids content is considered a reliable maturity index for many fruits, including bananas, and it is also related to the eating quality and sugar content. Generally, the sugars account for 80% of the SSC in fruits (Kader 2002). It would be of great interest to see a calibration model developed on a simple, cheap, and easy maintained device transferable to a more expensive and complex hyperspectral imaging system, when the distribution information of a target of interest is investigated.

Materials and Methods

Instruments

Due to availability of instruments, a portable micro NIR spectrometer (1700ES, Viavi Solutions Inc., USA) located in CREA-IT, Italy, and a benchtop NIR hyperspectral imaging system (DV s.r.l. Padova, Italy) located in UCD, Ireland, were employed for this study, as shown in Fig. 1a, b. The micro NIR spectrometer was considered as a master instrument (NIR-point, master); it has a physical scanner size of 1.6 cm in diameter. The hyperspectral imaging system was regarded as slave instrument (NIR-HSI, slave); it mainly consists of a spectrograph (N17E, SPECIM, Spectral Imaging Ltd., Finland), a camera (SU320M-1.7RT Sensors Unlimited, Inc., USA), and a diffusive illumination unit (190 W, halogen lights). Table 1 summarised details of the two instruments.

Bananito Samples

Ninety pairs of bananito fruit [*Musa acuminata* (AA)] in three maturity stages (stage 2, stage 4, and stage 6) were used in the study. The two connected fingers of each pair were carefully selected from the central position of the same hand. They had a very similar size, shape, and colour. Generally in the experiment of bananas, the whole banana hand is considered as a single element and evaluated as an experimental unit (Ahmad et al. 2001). The central connected fruits of the same hand develop from ovaries of connected flowers (Ram et al. 1962). They have the same history and start to develop at the same moment (Calabrese 1993). It is, then, very likely that the two connected fruits of the central part of each hand are exactly at the same maturity stage and that the maturity indices of these fruits are identical. Importantly, it was reported that soluble solids content (SSC) of bananas is less affected by the hand position when compared to than other maturity indices (Mustaffa et al. 1998). Therefore, the two fingers in each pair were considered as the same sample in this study.

To conduct the experiment, the two connected bananito fingers of each pair were labelled as 'finger-A' and 'finger-B', then they were separated accordingly. Finger-A fruits were kept in CREA-IT, Italy, for spectra acquisition using NIR-point instrument. Finger-B fruits were sent to University College Dublin (UCD), Ireland, by overnight express shipping for hyperspectral data acquisition using NIR-HSI instrument. It should be noted that finger-A fruits were kept in the same condition as finger-B fruits during the shipping time, and the experiments in CREA-IT and UCD were carried out at the same time.

Spectra Acquisition and SSC Measurement

Bananito fruits were cut lengthwise into two halves. NIR-point spectra were taken from two different locations on the same bananito flesh, as shown in Fig. 1c. The two NIR-point spectra were then averaged to generate a mean-spectrum to

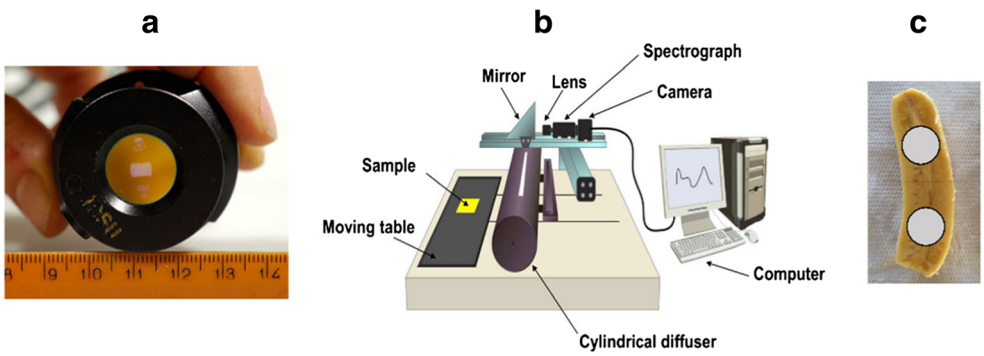

Fig. 1 Instruments and samples. **a** The handheld micro NIR spectrometer. **b** The line-scanned hyperspectral imaging system. **c** The two positions measured on bananito flesh by the micro NIR spectrometer

Table 1 Instrumental parameters of the micro NIR spectrometer and the hyperspectral imaging system

	Name	Spectral range recorded (nm)	Interval (nm)	No. of wavebands
Micro NIR spectrometer	NIR-point (master)	908–1676	6.2	125
Hyperspectral imaging	NIR-HSI (slave)	880–1720	7	121

represent each sample. NIR-HSI data was collected from hyperspectral imaging system by scanning the whole flesh-half for each sample. The mean-spectrum of each sample was obtained by averaging the spectra of all sample pixels.

The bananito halves of finger-B fruits were frozen for further determination of SSC. The SSC of each bananitos flesh was measured twice using a refractometer (RFM 81, Bellingham + Stanley, UK), using 5 g of the frozen sample homogenised with milliQ water at a ratio of 1:3 *w/w* (Blankenship et al. 1993). SSC values (%) were averaged per fruit.

Data Analysis

Data processing in the study was conducted using Matlab 2015a (The Math Works, Inc., USA) and PLS_toolbox 7.0 (Eigenvector Research, Inc., USA).

Dataset Splitting

A representative dataset is essential for a robust calibration model. There are a number of methods for selection of calibration samples, whereas the Kennard-Stone (KS) algorithm proposed by Kennard and Stone (1969) is popular and being widely used for uniform subset selection. The key of KS algorithm is to select calibration samples that are evenly distributed over the dataset with data points at both extremes included. Thus, a model with better predictive performance can be achieved (Perez-Guaita et al. 2012, Stanimirova et al. 2008). It works as follows: (a) the two samples with the largest geometric distance were first to be selected in the calibration set. The distance between two samples (p and q) can be calculated based on their spectra (x_p and x_q) using Euclidean distances (Galvão et al. 2005) as shown in Eq. 1.

$$E_{distance}(p,q) = \sqrt{\sum_{j=1}^{n}\left[x_p(j) - x_q(j)\right]^2} \quad (1)$$

where x_p and x_q are the spectrum vectors of sample p and sample q, x(j) is the reflectance response at the j-th waveband, and n is the total number of wavebands.

(b) The next candidate to be chosen as a calibration sample is the one that has the greatest separation distance from those already being selected. (c) The second step is repeated until the calibration set reaches the required number.

In the study, the KS algorithm was applied on 90 SNV pre-processed NIR-point spectra collected from the master instrument. The number of samples in the calibration, standardization, and validation set was 65, 10, and 15, respectively.

Spectra Interpolation and Pre-processing

To enable standardization, it is important that the spectra collected from both master and slave instruments have the same spectral range and interval. To achieve this, the first step was to trim the spectra to a common range. In this study, the spectral region from 939 to 1602 nm was investigated. Secondly, spectral interpolation was performed on the slave spectra using a cubic spline interpolation. Thus, after spectral trimming and interpolation, the NIR-HSI spectra had the same spectral resolution (6.2 nm) and number of wavelengths (108 wavebands) as the NIR-point spectra.

Spectral pre-treatments such as SNV, MSC, and derivative were implemented on the spectra of ten standardization samples. Spectral differences between master and slave instruments were calculated to select an optimal pre-treatment method that could maximise the similarity between both spectra.

Calculation of Spectral Difference

To evaluate how different the slave spectra (**X2,** $m \times n$) were from the master spectra (**X1,** $m \times n$), the spectral difference (Spe_Diff, %) was calculated using Eq. 2.

$$\text{Spe\_}Diff\ (\%) = \frac{\sqrt{\sum\left[(\boldsymbol{X}1)_{i,j} - (\boldsymbol{X}2)_{i,j}\right]^2}}{\sqrt{\sum(\boldsymbol{X}1)_{i,j}^2}} \times 100 \qquad (i = 1\ldots m; j = 1\ldots n) \quad (2)$$

where **X1** and **X2** were a $m \times n$ spectra matrix from master and slave instrument, respectively. m is the number of samples and n is the number of wavelengths. $\mathbf{X}_{i,j}$ is the reflectance response of the i-th and j-th element of the matrix.

Standardization Methods

Spectral standardization was implemented on spectra of the ten transfer samples that were measured by both master and slave instrument, respectively. Direct standardization (DS)

and piecewise direct standardization (PDS) were employed to correct the slave spectra. In PDS, the relative reflectance intensity at the *j*-th wavelength in the master spectra matrix (**X1**(*j*)) was correlated to the corresponding *j*-th wavelength of the slave spectra matrix and its adjacent neighbours (**X2**([*j*-*z*,...,*j*,...,*j* + *z*])) located in a pre-defined moving window, where *z* is defined by the window size (*w*, *w* = 2*z* + 1). The partial least squares regression (PLSR) was performed between **X1**(*j*) and **X2**([*j*-*z*,...,*j*,...,*j* + *z*]) to calculate the regression coefficients **b**(*j*) for each wavelength *j*, as shown in Eq. 3.

$$\mathbf{X1}(j) = \mathbf{X2}([j-z, \ldots, j, \ldots, j+z]) \cdot \mathbf{b}(j) + \mathbf{b}_0(j) \quad (3)$$

where **X1** and **X2** were the spectra matrix of standardization samples obtained from master and slave instrument, and $\mathbf{b_0}(j)$ was the offset at the *j*-th wavelength.

A transfer matrix **F** consisting of the regression coefficient vectors **b**(*j*) from all wavelengths was generated. It was subsequently used to standardize spectra of new samples measured by the slave instrument $\mathbf{X2_{new}}$. Calculation of those standardized spectra $(\mathbf{X2_{new}})_{std}$ was presented in Eq. 4.

$$(\mathbf{X2_{new}})_{\mathrm{std}} = \mathbf{X2_{new}} \times \mathbf{F} + \mathbf{b}_0 \quad (4)$$

where $\mathbf{b_0}$ was a matrix containing the offsets at all wavelengths. More details on the PDS algorithm can be found in Ji et al. (2015).

Figure 2 displayed the difference between DS and PDS in a graphical way. The blue spectrum on the top was the mean-spectrum of the ten transfer samples obtained by NIR-point, and the green spectrum at the bottom was the mean-spectrum of the ten transfer samples obtained by NIR-HSI. The main difference between DS and PDS is that the DS method works on the full spectral region, whereas the PDS method works with a moving window.

Model Transfer Process

The calibration transfer process in the study is presented in Fig. 3. (1) A PLS calibration model was developed using the spectra from NIR-point master instrument to predict SSC of bananito flesh; cross-validation (CV) was performed using Venetian blinds (data splits = 8). (2) A standardization method was developed with the ten samples in the standardization (Std) set. (3) The optimal standardization method was applied to the slave spectra of 15 independent validation samples to generate corresponding standardized slave spectra. (4) The developed PLS model was applied to the 15 standardized slave spectra to predict SSC of the validation samples. (5) After spectra and images processing in the hyperspectral data, the developed PLS model was applied to hypercubes in a pixelwise manner to generate SSC distribution maps of bananito flesh.

Results and Discussion

Removal of Bad Pixels from Hyperspectral Images

The original hyperspectral images included spectral and spatial information of background and bananito flesh. To

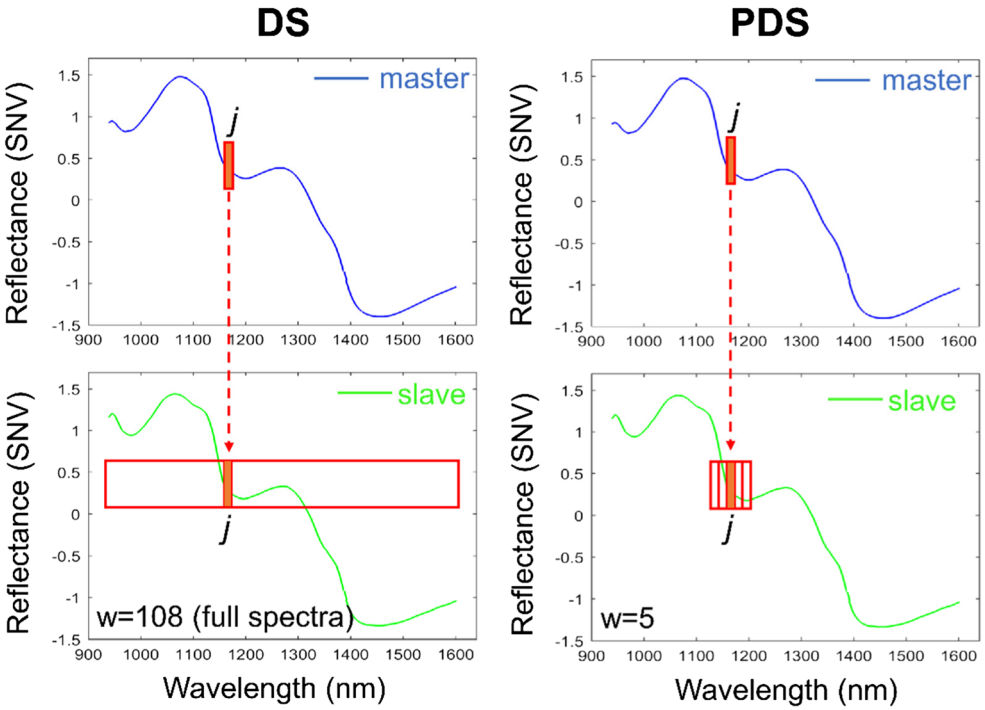

Fig. 2 Graphical view of direct standardization (DS) and piecewise direct standardization (PDS)

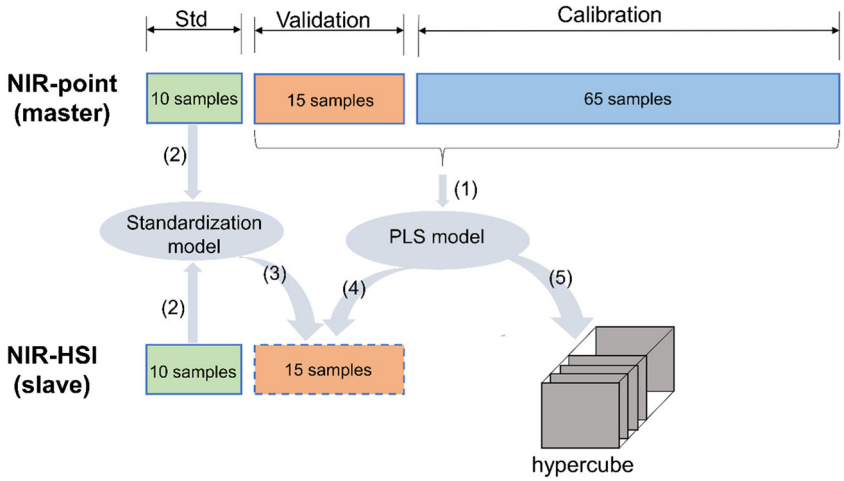

Fig. 3 Calibration transfer from NIR-point to NIR-HSI instrument flow chart

remove the background from the region of interests, a simple and effective method called thresholding was conducted on images at the wavelength of 1069 nm, where a strong contrast in spectral intensity between flesh sample and the background was displayed. A histogram graph showing the distribution of the intensity value of all pixels was plotted to find a threshold for segmentation. In the study, an optimal threshold value of 0.135 was selected as a mark-off to generate a binary mask so as to differentiate the sample from the background. Thus, the raw spectra of all pixels belonged to the sample can be extracted.

In NIR hyperspectral imaging, it has been reported that typically around 1% of pixels are unreliable due to instrumental artefacts in the detector (Firtha et al. 2008). It is important to examine the hyperspectral images and to eliminate those 'bad' pixels that might affect the accuracy of modelling and mapping (Vidal and Amigo 2012). The spectral profile of pixels belonging to a bananito flesh sample is shown in Fig. 4. When looking over the raw reflectance spectra (Fig. 4a), some abnormal spectra with sharp peaks were observed. SNV pre-treatment was applied to the raw spectra, as shown in Fig. 4b, more abnormal peaks were observed. This is because SNV transformed each spectrum to mean zero and standard deviation of one. As a result, the abnormal signals along the spectrum were amplified. To identify these bad pixels, the image at each wavelength of an $x \times y \times \lambda$ hypercube (hypercube-raw, x and y represent the two-

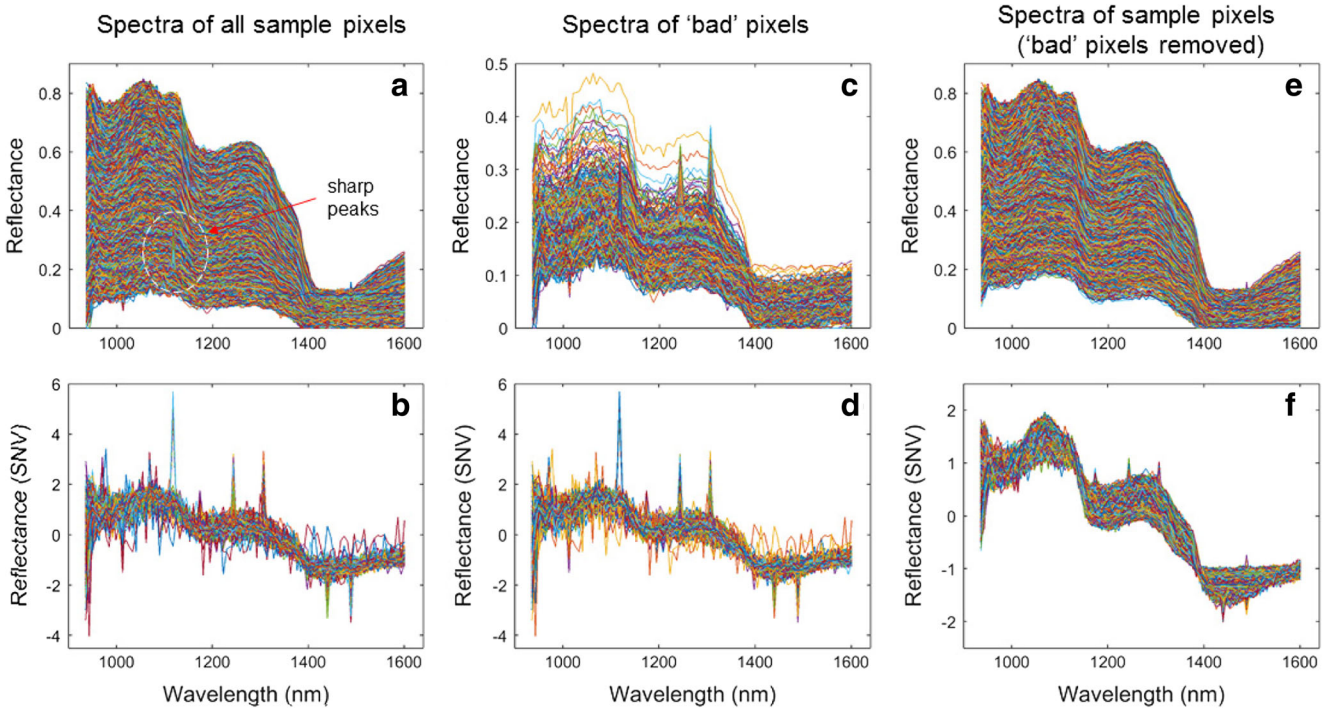

Fig. 4 Spectral profiles of all sample pixels, 'bad' pixels with unexpected signals, and pixels with removal of the 'bad' ones. **a**, **c,** and **e** were the raw spectra; **b**, **d,** and **f** were the SNV pre-treated spectra

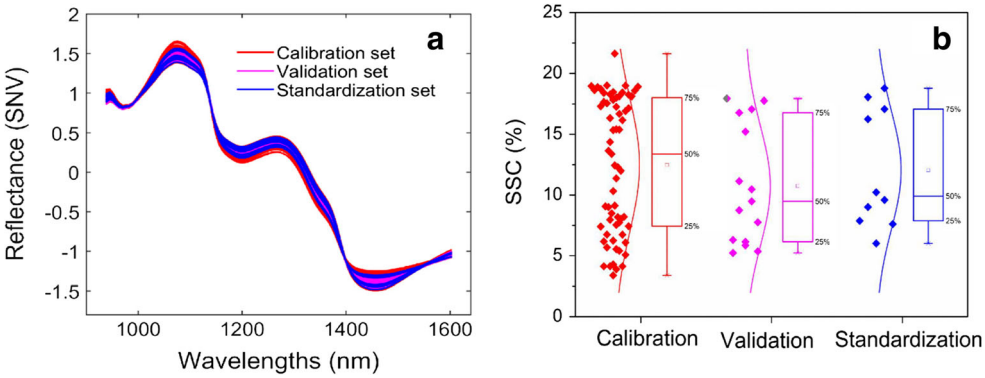

Fig. 5 Data variations in calibration, validation and standardization set. **a** Spectra variations. **b** SSC variations

dimensional spatial information, λ represents the wavelength) was subtracted by the next image, resulting in an $x \times y \times (\lambda\text{-}1)$ hypercube (hypercube-diff) with each slice showing the intensity difference between the two adjacent wavelength images. Standard deviation was calculated at each pixel of the hypercube-diff, pixels that had a high standard deviation were identified as bad pixels. Figure 4c, d presented the raw and SNV-pretreated spectra of bad pixels. Figure 4e, f showed the raw and SNV-pre-treated spectra of bananito pixels with removal of bad pixels. Comparing Fig. 4b, f, it was obvious that bad pixels with very unusual spectral readings were successfully detected and removed using the abovementioned image-processing strategy. While there were still some small noisy peaks in the spectra of Fig. 4f, it was removed by Savitzky-Golay smoothing algorithm with a window width of 5, polynomial order of 2, and derivative order of 0.

Dataset Variations

Partition of samples for multivariate calibration and transfer needs to take two aspects into consideration. On the one hand, the calibration set should cover all possible variance among samples, and as a result, new samples can be well predicted by the model. On the other hand, the validation set and standardization set should be completely independent from the calibration set and evenly distributed along the calibration space; this avoids overestimating the model performance. Figure 5 shows data variations in calibration, validation, and standardization sets. As shown in Fig. 5a, the spectral variabilities in validation and standardization sets were included in the range of calibration samples. This was expected since the KS algorithm used for sample partition was based on spectral information alone (Galvão et al. 2005). The result of SSC analysis

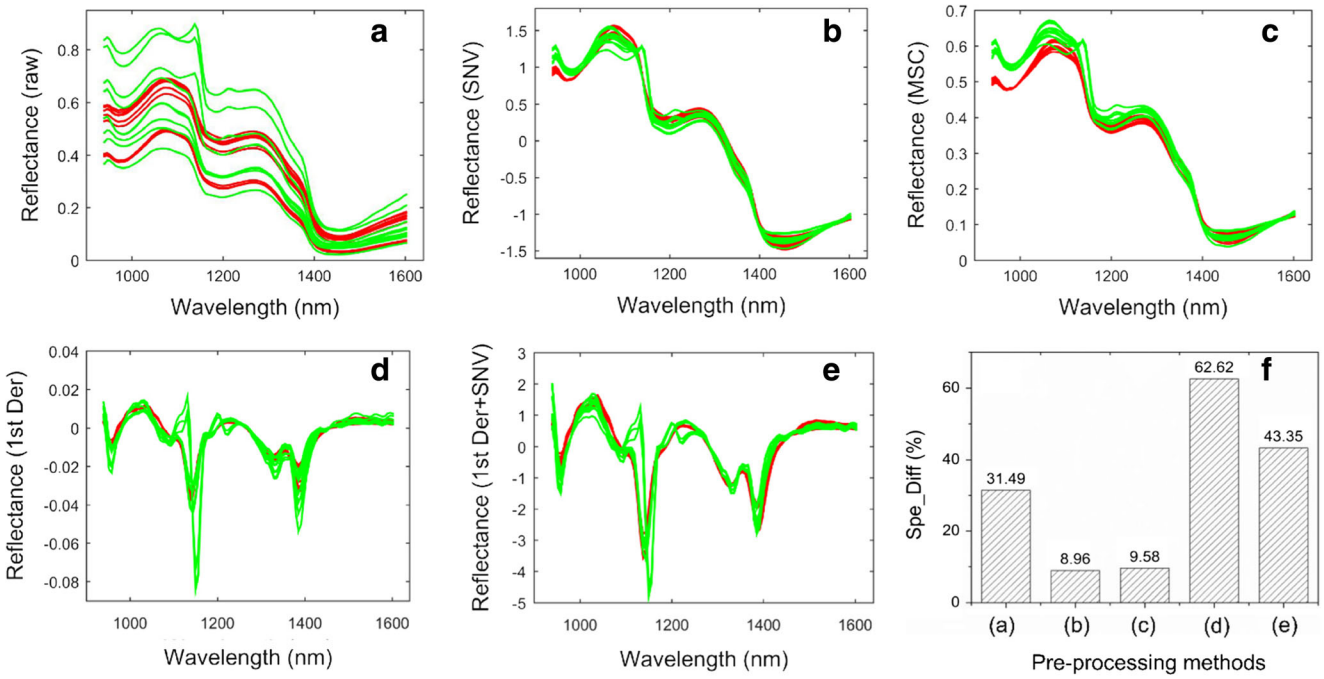

Fig. 6 Spectral profiles of raw and pre-processed spectra of the ten standardization samples acquired by micro NIR spectrometer (NIR-point, the red spectra) and NIR hyperspectral imaging (NIR-HSI, the green spectra). **a** Raw spectra. **b** SNV. **c** MSC. **d** First-derivative (1st Der, window size = 5, order = 2). **e** 1st Der + SNV. **f** Comparison of spectral difference using different pre-treatment methods

is shown in Fig. 5b. The SSC value of bananito flesh in calibration set ranged from 3.38 to 21.62%, whereas the SSC value of bananito flesh in validation and standardization sets varied from 5.22 to 17.94% and from 6.01 to 18.77%, respectively. It was obvious that data variances in validation and standardization set were covered by the calibration set with respect to either spectra or SSC, illustrating that the KS algorithm used in the study was an effective method for dataset selection.

Spectral Pre-processing

The use of appropriate spectral pre-processing can make calibration models more transferable (Soldado et al. 2013). In the study, several pre-processing methods were applied to the raw spectra of ten transferable samples analysed by the master and slave instrument. Spectral difference between NIR-point spectra and NIR-HSI spectra was calculated to find an optimal pre-processing method for calibration transfer. Figure 6a–e shows the spectral profiles of NIR-point and NIR-HSI before and after selected pre-treatments. A significant difference was observed in the raw mean spectra of NIR-point and NIR-HIS, as shown in Fig. 6a. In addition, both NIR-point and NIR-HSI spectra had a large scattering effect in the spectral region of 939–1380 nm. Feature absorbance bands located at around 970 and 1187 nm were corresponding to O–H and C–H stretching second overtone, respectively, due to a large amount of water and carbohydrates presented in bananitos flesh. A relatively broad absorbance band was seen in the spectral region of 1400–1500 nm that is related to the overlap of several NIR absorption bands due to different vibrations of chemical bonds, i.e. O–H and C–H (Osborne 2006). After SNV pre-treatment, the scaling differences arise from light scattering or different pathlengths were significantly reduced (Fig. 6b), and the NIR-point and NIR-HSI spectra with SNV pre-treatment had a similar spectral profile. Nevertheless, some NIR-HSI spectra had a relatively higher reflectance value at wavelengths of 1137 and 1212 nm, which might be due to the fact that hyperspectral imaging captured more spatial information from bananitos flesh comparing with micro NIR spectrometer. Figure 6c shows the result of MSC pre-treatment. When compared with the spectra after SNV, the NIR-point and NIR-HSI spectra showed a significant difference in the spectral range of 936–1150 nm. Transforming the raw spectra to the first-derivative (1st Der) spectra was implemented using Savitzky-Golay smoothing algorithm with a window size of 5 and polynomial order of 2, and the result is shown in Fig. 6d. Derivatives attempted to reduce the multiplicative scatter effects. However, a more complex spectral profile was obtained as derivatives enhanced peak signals and at the meanwhile enlarged the spectral difference at 1137 and 1212 nm, which might diminish the transformability of calibration model (Fearn 2001). A combined pre-processing of 1st Der followed by SNV was applied to the raw mean spectra and the resule is shown in Fig. 6e. Similar to 1st Der, the NIR-point spectra and NIR-HSI spectra did not match very well particularly at wavelengths of 1137 and 1212 nm. The spectral difference for each pre-treatment was calculated and the result is shown in Fig. 6f. The application of SNV to raw spectra yielded a remarkable result by decreasing the spectral difference from 34.49 to 8.96%. Therefore, SNV was selected as an optimal pre-processing method in the study in terms of data difference reduction.

Calibration Transfer

Development of a PLS Calibration Model

A PLS calibration model was developed using the 65 mean spectra (SNV pre-treated) from the master instrument. Model details are shown in Fig. 7. The number of latent variables (LVs) was selected according to the RMSE value in the cross-validation. As shown in Fig. 7a, four latent variables were selected since the changes in RMSE value were small after four LVs. Selection of more LVs might cause model overfitting. The plot of measured SSC and predicted SSC is shown in Fig. 7b. The calibration sample (in grey colour) and validation samples (in red colour) were evenly distributed along the 1:1 line, indicating the model yielded a high prediction performance, with coefficient of determination (R^2) of

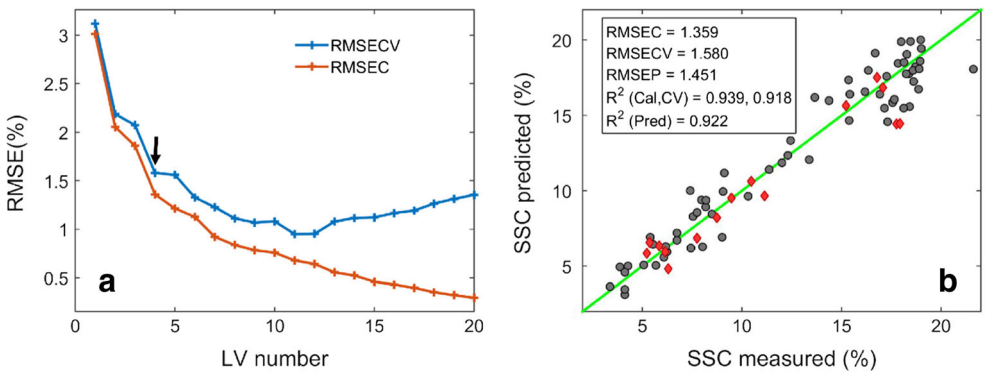

Fig. 7 The PLS model developed on the master instrument for predicting SSC of bananitos flesh. **a** Selection of the optimal number of latent variables. **b** Predicted versus measured SSC of calibration set (in grey colour) and validation set (in red colour)

0.939, 0.918, and 0.922 and root mean square error (RMSE) of 1.359%, 1.580%, and 1.451% for calibration, cross-validation, and validation, respectively. The prediction bias, slope, and RDP (the ratio of standard deviation to RMSEP) of the calibration model were − 0.534, 0.865, and 3.38, respectively.

Comparison of standardization Methods

After SNV pre-processing, different standardization methods based on DS and PDS algorithms were developed using the NIR-point and NIR-HSI spectra of the ten standardization samples. Each standardization method was applied to the NIR-HSI spectra of the 15 validation samples for spectra correction. Then, the developed calibration model was applied to the 15 standardized NIR-HSI spectra for SSC prediction. The success of the calibration transfer was evaluated by the prediction accuracy in terms of R^2 and RMSE.

The calibration transfer results for predicting SSC of validation samples are summarised in Table 2. The direct use of the developed calibration model to the slave instrument was impracticable in this case, yielding a poor prediction accuracy (RMSEP = 35.83%), since there was a large spectral difference (9.18%) remaining between NIR-point and NIR-HIS spectra. When the slave spectra NIR-HSI were standardized by different standardization methods, the predictability of the calibration model was remarkably improved in decreasing the spectral differences and RMSEP as well as increasing the R^2_p. With the use of DS standardization, the spectral difference was decreased from 9.18 to 3.64%, yielding a predictive accuracy of R^2_p = 0.761 and RMSEP = 2.662%. PDS methods as affected by different window sizes were investigated. In PDS, the spectral difference between NIR-point and NIR-HSI (after standardization) increased with increasing the window size. As a result, the corresponding R^2_p decreased from 0.925 to 0.810 and RMSEP increased from 1.952 to 2.410% when the window size changed from 3 to 11, respectively. Overall, the best standardization method was PDS with a window size of 3, yielding an equivalent SSC prediction accuracy of R^2_p = 0.925 and RMSEP = 1.592% when compared with the results achieved by using NIR-point spectra of validation samples (R^2_p = 0.922 and RMSEP = 1.451%).

Figure 8 shows the spectral difference throughout the entire wavelength range before and after PDS (window size = 3) standardization was applied on the slave spectra of the 15 validation samples. As can be seen from the pre-standardization spectral difference, SNV pre-treatment could not eliminate all spectral differences between master and slave spectra. Particularly, the spectral differences at wavelengths of 1100–1200 nm were significantly larger than other wavelengths. However, after the application of PDS (window size = 3) to NIR-HSI spectra, the remaining spectral differences reduced to a relatively small value. Variations in post-standardization spectral differences were levelled off. The results demonstrated that the use of additional standardization method is capable of narrowing the spectral differences that could not be removed by pre-treatments. Thus, calibration models are more transferable.

SSC Distribution

One of the main advantages of hyperspectral imaging is to provide spatial information that shows the distribution of target properties on the sample. In the study, the developed PLS model was applied to the spectra of all sample pixels in the hyperspectral datacube after image processing, SNV pre-treatment, and PDS standardization (window size = 3). As a result, a prediction map can be generated to show the distribution of SSC.

Three bananitos samples (B1, B2, and B3) at different ripening levels (the measured SSC (SSC_m) = 4.12, 10.47, and 17.07%, respectively) were selected to show SSC distribution on the flesh, and the result is presented in Fig. 9a. A colour scale (displayed on the right-hand side of the figure) changes from blue to yellow, which is corresponding to changes of SSC from 0 to 30%. After calibration transfer, the predicted SSC (SSC_p) for these three samples was 5.47, 8.98, 16.38%, respectively. The SSC variations between measured and predicted values were within the prediction error of the calibration model (RMSEP = 1.592%). The results demonstrated that

Table 2 Comparison of different standardization methods for predicting SSC of validation samples

Standardization method	Window size	Spectral difference[a] (%)	R^2_p	RMSEP (%)
No standardization	108	9.18	0	35.83
DS[b]	108	3.64	0.761	2.662
PDS[c]	3	2.82	0.925	1.592
PDS	7	2.92	0.871	2.185
PDS	11	3.03	0.810	2.41

[a] Spectral difference is calculated between NIR-point spectra (after SNV pre-treatment) and NIR-HSI spectra (after SNV pre-treatment and with/without standardization) of the 15 validation samples

[b] DS direct standardization

[c] PDS piecewise direct standardization

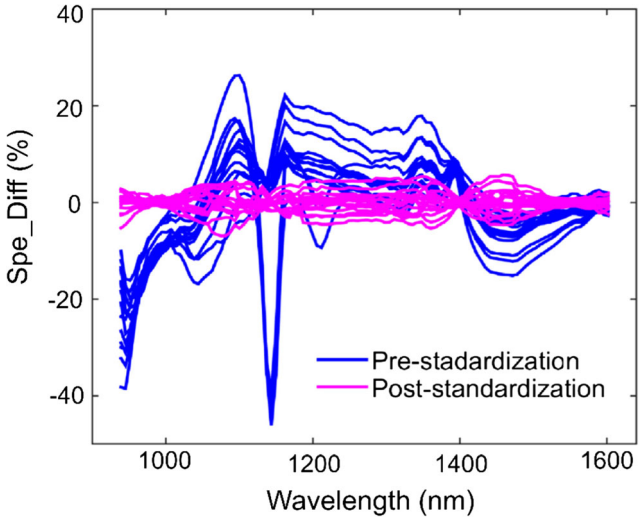

Fig. 8 Spectral difference throughout the entire wavelength range before and after PDS (window size = 3) standardization was applied on the slave spectra of the 15 validation samples

the PLS calibration model was transferable from the micro NIR spectrometer to hyperspectral imaging to visualise SSC distributions on bananito flesh.

By an overall view of the colour distribution on the flesh, it is observed that more blue colour is presented on the B1 sample, whereas more yellow colour is presented on the B3 sample, indicating that a low soluble solids content in B1 and a high soluble solids content in B3. This result can be explained by the degradation of starch into soluble sugars during banana ripening, which is a major biochemical change occurred in the flesh. The starch-iodine test of three bananito samples at similar ripening stages is shown in Fig. 9b, demonstrating the decrease of starch and the increase of SSC in bananito flesh when the fruit ripens.

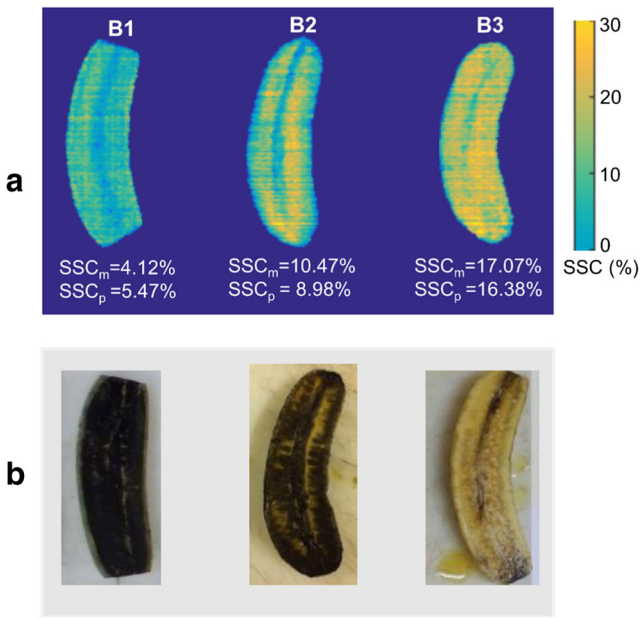

Fig. 9 SSC distribution maps on bananito samples after calibration transfer (**a**); starch-iodine test on bananito samples (**b**)

A bananito fruit consists of exocarp (peel), mesocarp (pulp/flesh), and endocarp (inner part). The endocarp, also edible, consists of the placental axis (central part that develops from the placental tissue of the flower) and the epithelial tissue that rounds the aborted seeds (Robinson and Saúco 2010). During banana ripening, the conversion of starch into sugars involves several enzymes (amylase, glucosidase, sucrose synthase, and sucrose phosphate synthase). This process starts from the epithelial tissue of the endocarp and then radiated towards the ends of the transversally cut fruit (Blankenship et al. 1993, Cordenunsi and Lajolo 1995). This phenomenon is clearly displayed on the prediction maps of B2 and B3, where the yellow colour extends from interior to edge with increasing the ripeness levels.

Conclusions and Future Work

The application of SNV pre-processing combined with PDS (window size = 3) standardization showed the best calibration transfer performance in remarkably decreasing the spectral differences between the spectra from the master and the slave instruments. The PLS calibration model established on the micro NIR spectrometer performed well on spectra acquired from the hyperspectral imaging. SSC prediction maps generated from the calibration model showed that the cut bananitos had a lower SSC along the central line, and SSC increased from the interior to the edge when ripening. This study proved the feasibility of transferring calibration models from spectrometers to hyperspectral imaging. In future applications, calibration models developed by a simple handheld micro spectrometer can further be applied to hyperspectral imaging spectra, particularly when spatial information on the sample is studied.

Further investigations to improve the transferability of calibration models could be focused on (1) to include more samples with a large SSC variation for calibration development, (2) to apply feature wavelength selection strategies to reduce computation time and simplify the calibration procedure, and (3) to consider more advanced spectral pre-treatments and standardizations and their combinations for spectral correction, thus minimising the spectral difference between master and slave instruments.

Acknowledgments The authors would like to greatly acknowledge PhD students Le Wen, Kexin Zhang, and Sindhuraj Mukherjee, and the research group of Prof. Colm O'Donnell from School of Biosystems and Food Engineering, UCD for their help in image acquisition of bananitos using NIR-HSI system. The authors would also like to thank Annamaria Stellari for technical support and the AL.MA s.r.l. company for bananito fruit supply. UCD-CSC Scholarship Scheme supported by University

College Dublin (UCD) and China Scholarship Council (CSC) was acknowledged for this study.

Compliance with Ethical Standards

Conflict of Interest Yuan-Yuan Pu declares that she has no conflict of interest. Da-Wen Sun declares that he has no conflict of interest. Cecilia Riccioli declares that she has no conflict of interest. Marina Buccheri declares that she has no conflict of interest. Maurizio Grassi declares that he has no conflict of interest. Tiziana M.P. Cattaneo declares that she has no conflict of interest. Aoife Gowen declares that she has no conflict of interest.

Ethical Approval This article does not contain any studies with human participants performed by any of the authors.

Informed Consent Not applicable.

References

Ahmad S, Clarke B, Thompson A (2001) Banana harvest maturity and fruit position on the quality of ripe fruit. Ann Appl Biol 139:329–335

Amigo JM, Babamoradi H, Elcoroaristizabal S (2015) Hyperspectral image analysis. A tutorial. Anal Chim Acta 896:34–51

Antonucci F, Pallottino F, Paglia G, Palma A, D'Aquino S, Menesatti P (2011) Non-destructive estimation of mandarin maturity status through portable VIS-NIR spectrophotometer. Food Bioprocess Technol 4:809–813

Blankenship SM, Ellsworth DD, Powell RG (1993) A ripening index for banana fruit based on starch content. HortTechnology 3:338–339

Bouveresse E, Hartmann C, Massart DL, Last IR, Prebble KA (1996) Standardization of near-infrared spectrometric instruments. Anal Chem 68:982–990

Calabrese, F. 1993. Frutticoltura tropicale e subtropicale I: fruttiferi erbacei e suffruticosi

Cheng J-H, Sun D-W (2015a) Rapid and non-invasive detection of fish microbial spoilage by visible and near infrared hypersZpectral imaging and multivariate analysis. Lwt-Food Science And Technology 62:1060–1068

Cheng J-H, Sun D-W (2017) Partial Least Squares Regression (PLSR) Applied to NIR and HSI Spectral Data Modeling to Predict Chemical Properties of Fish Muscle. Food Engineering Reviews 9: 36–49

Cheng J-H, Sun D-W, Pu H, Zhu Z (2015b) Development of hyperspectral imaging coupled with chemometric analysis to monitor K value for evaluation of chemical spoilage in fish fillets. Food Chemistry 185:245–253

Cheng J-H, Sun D-W, Pu H (2016a) Combining the genetic algorithm and successive projection algorithm for the selection of feature wavelengths to evaluate exudative characteristics in frozen-thawed fish muscle. Food Chemistry 197:855–863

Cheng J-H, Sun D-W, Qu J-H, Pu H-B, Zhang X-C, Song Z, Chen X, Zhang H (2016b) Developing a multispectral imaging for simultaneous prediction of freshness indicators during chemical spoilage of grass carp fish fillet. Journal of Food Engineering 182:9–17

Cheng L, Sun D-W, Zhu Z, Zhang Z (2017) Emerging techniques for assisting and accelerating food freezing processes: A review of recent research progresses. Critical Reviews In Food Science and Nutrition 57:769–781

Cordenunsi BR, Lajolo FM (1995) Starch breakdown during banana ripening: sucrose synthase and sucrose phosphate synthase. J Agric Food Chem 43:347–351

Delgado AE, Sun D-W (2002) Desorption isotherms and glass transition temperature for chicken meat Journal Of Food Engineering Vol 55: 1–8

Du CJ, Sun D-W (2005) Pizza sauce spread classification using colour vision and support vector machines. Journal of Food Engineering Vol 66:137–145

Elmasry G, Sun D-W (2010) CHAPTER 1—principles of hyperspectral imaging technology. In: Sun D-W (ed) Hyperspectral imaging for food quality analysis and control. Academic Press, San Diego

ElMasry G, Sun D-W, Allen P (2013) Chemical-free assessment and mapping of major constituents in beef using hyperspectral imaging. Journal of Food Engineering 117:235–246

Fearn T (2001) Standardisation and calibration transfer for near infrared instruments: a review. J Near Infrared Spectrosc 9:229–244

Feng Y-Z, Sun D-W (2013a) Near-infrared hyperspectral imaging in tandem with partial least squares regression and genetic algorithm for non-destructive determination and visualization of Pseudomonas loads in chicken fillets. Talanta 109:74–83

Feng Y-Z, ElMasry G, Sun D-W, Scannell Amalia GM, Des W, Morcy N (2013b) Near-infrared hyperspectral imaging and partial least squares regression for rapid and reagentless determination of Enterobacteriaceae on chicken fillets. Food Chemistry 138:1829–1836

Feudale RN, Woody NA, Tan H, Myles AJ, Brown SD, Ferré J (2002) Transfer of multivariate calibration models: a review. Chemom Intell Lab Syst 64:181–192

Firtha F, Fekete A, Kaszab T, Gillay B, Nogula-nagy M, Kovács Z, Kantor DB (2008) Methods for improving image quality and reducing data load of NIR hyperspectral images. Sensors (Basel, Switzerland) 8:3287–3298

Galvão RKH, Araujo MCU, José GE, Pontes MJC, Silva EC, Saldanha TCB (2005) A method for calibration and validation subset partitioning. Talanta 67:736–740

Ge Y, Morgan CLS, Grunwald S, Brown DJ, Sarkhot DV (2011) Comparison of soil reflectance spectra and calibration models obtained using multiple spectrometers. Geoderma 161:202–211

Gendrin C, Roggo Y, Collet C (2008) Pharmaceutical applications of vibrational chemical imaging and chemometrics: a review. J Pharm Biomed Anal 48:533–553

Gowen AA, O'Donnell CP, Cullen PJ, Downey G, Frias JM (2007) Hyperspectral imaging—an emerging process analytical tool for food quality and safety control. Trends Food Sci Technol 18:590–598

Grelet C, Fernández Pierna JA, Dardenne P, Baeten V, Dehareng F (2015) Standardization of milk mid-infrared spectra from a European dairy network. J Dairy Sci 98:2150–2160

Huang J, Romero-Torres S, Moshgbar M (2010) Practical considerations in data pre-treatment for NIR and Raman spectroscopy. Am Pharm Rev 13:116–127

Jackman P, Sun D-W, Allen P (2009) Automatic segmentation of beef longissimus dorsi muscle and marbling by an adaptable algorithm. Meat Science 83:187–194

Jackman P, Sun D-W, Allen P (2011) Recent advances in the use of computer vision technology in the quality assessment of fresh meats. Trends In Food Science & Technology 22:185–197

Ji W, Viscarra Rossel RA, Shi Z (2015) Improved estimates of organic carbon using proximally sensed vis–NIR spectra corrected by piecewise direct standardization. Eur J Soil Sci 66:670–678

Kader AA (2002) Postharvest technology of horticultural crops, University of California, Agric Nat Resour

Kamruzzaman M, ElMasry G, Sun D-W, Allen P (2013) Non-destructive assessment of instrumental and sensory tenderness of lamb meat using NIR hyperspectral imaging. Food Chemistry 141:389–396

Kennard RW, Stone LA (1969) Computer aided design of experiments. Technometrics 11:137–148

Kiani H, Zhang Z, Delgado A, Sun D-W (2011) Ultrasound assisted nucleation of some liquid and solid model foods during freezing. Food Research International 44:2915–2921

Li J-L, Sun D-W, Pu H, Jayas DS (2017) Determination of trace thiophanate-methyl and its metabolite carbendazim with teratogenic risk in red bell pepper (Capsicumannuum L.) by surface-enhanced Raman imaging technique. Food Chemistry 218:543–552

Liang C, Yuan H-F, Zhao Z, Song C-F, Wang J-J (2016) A new multivariate calibration model transfer method of near-infrared spectral analysis. Chemom Intell Lab Syst 153:51–57

Liu Z, Yu H, Macgregor JF (2007) Standardization of line-scan NIR imaging systems. J Chemom 21:88–95

Liu Y, Cai W, Shao X (2014) Standardization of near infrared spectra measured on multi-instrument. Anal Chim Acta 836:18–23

Liu D, Ma J, Sun D-W, Pu H, Gao W, Qu J, Zeng X-A (2014) Prediction of color and pH of salted porcine meats using visible and near-infrared hyperspectral imaging. Food Bioprocess Technol 7(11): 3100–3108

Lorente D, Aleixos N, Gómez-Sanchis J, Cubero S, García-Navarrete OL, Blasco J (2012) Recent advances and applications of hyperspectral imaging for fruit and vegetable quality assessment. Food Bioprocess Technol 5(4):1121–1142

Luypaert J, Massart DL, Vander Heyden Y (2007) Near-infrared spectroscopy applications in pharmaceutical analysis. Talanta 72:865–883

Ma J, Pu H, Sun D-W, Gao W, Qu J-H, Ma K-Y (2015) Application of Vis-NIR hyperspectral imaging in classification between fresh and frozen-thawed pork Longissimus Dorsi muscles. International Journal of Refrigeration-Revue Internationale Du Froid 50:10–18

Ma J, Sun D-W, Pu H (2016) Spectral absorption index in hyperspectral image analysis for predicting moisture contents in pork longissimus dorsi muscles. Food Chemistry 197:848–854

Ma J, Sun D-W, Qu J-H, Pu H (2017) Prediction of textural changes in grass carp fillets as affected by vacuum freeze drying using hyperspectral imaging based on integrated group wavelengths. Lwt-Food Science and Technology 82:377–385

McDonald K, Sun D-W, Kenny T (2000) of the quality of cooked beef products cooled by vacuum cooling and by conventional cooling. Lebensmittel-Wissenschaft Und-Technologie-Food Science and Technology Vol 33:21–29

McDonald K, Sun D-W, Kenny T (2001) The effect of injection level on the quality of a rapid vacuum cooled cooked beef product. Journal of Food Engineering Vol 47:139–147

Mustaffa R, Osman A, Yusof S, Mohamed S (1998) Physico-chemical changes in Cavendish banana (Musa cavendishiiL var Montel) at different positions within a bunch during development and maturation. J Sci Food Agric 78:201–207

Nicolaï BM, Beullens K, Bobelyn E, Peirs A, Saeys W, Theron KI, Lammertyn J (2007) Nondestructive measurement of fruit and vegetable quality by means of NIR spectroscopy: a review. Postharvest Biol Technol 46:99–118

Oliveri P, Casolino MC, Casale M, Medini L, Mare F, Lanteri S (2013) A spectral transfer procedure for application of a single class-model to spectra recorded by different near-infrared spectrometers for authentication of olives in brine. Anal Chim Acta 761:46–52

Osborne BG (2006) Near-infrared spectroscopy in food analysis. John Wiley & Sons, Ltd., Encyclopedia of Analytical Chemistry

Pereira CF, Pimentel MF, Galvao RK, Honorato FA, Stragevitch L, Martins MN (2008) A comparative study of calibration transfer methods for determination of gasoline quality parameters in three different near infrared spectrometers. Anal Chim Acta 611:41–47

Pereira LSA, Carneiro MF, Botelho BG, Sena MM (2016) Calibration transfer from powder mixtures to intact tablets: a new use in pharmaceutical analysis for a known tool. Talanta 147:351–357

Perez-Guaita D, Ventura-Gayete J, Pérez-Rambla C, Sancho-Andreu M, Garrigues S, De La Guardia M (2012) Protein determination in serum and whole blood by attenuated total reflectance infrared spectroscopy. Anal Bioanal Chem 404:649–656

Pierna JAF, Vermeulen P, Lecler B, Baeten V, Dardenne P (2010) Calibration transfer from dispersive instruments to handheld spectrometers. Appl Spectrosc 64:644–648

Pojić MM, Mastilović JS (2013) Near infrared spectroscopy—advanced analytical tool in wheat breeding, trade, and processing. Food Bioprocess Technol 6:330–352

Pu Y-Y, Sun D-W (2016) Prediction of moisture content uniformity of microwave-vacuum dried mangoes as affected by different shapes using NIR hyperspectral imaging. Innovative Food Science & Emerging Technologies 33:348–356

Pu Y-Y, Sun D-W (2017) Combined hot-air and microwave-vacuum drying for improving drying uniformity of mango slices based on hyperspectral imaging visualisation of moisture content distribution. Biosystems Engineering 156:108–119

Pu H, Sun D-W, Ma J, Cheng J-H (2015a) Classification of fresh and frozen-thawed pork muscles using visible and near infrared hyperspectral imaging and textural analysis. Meat Science 99:81–88

Pu H, Kamruzzaman M, Sun D-W (2015b) Selection of feature wavelengths for developing multispectral imaging systems for quality, safety and authenticity of muscle foods-a review. Trends In Food Science & Technology 45:86–104

Qin Y, Gong H (2016) NIR models for predicting total sugar in tobacco for samples with different physical states. Infrared Phys Technol 77: 239–243

Qu J-H, Sun D-W, Cheng J-H et al (2017) Mapping moisture contents in grass carp (Ctenopharyngodon idella) slices under different freeze drying periods by Vis-NIR hyperspectral imaging. lwt-food science and technology 75:529–536

Ram HM, Ram M, Steward F (1962) Growth and development of the banana plant: 3. A. The origin of the inflorescence and the development of the flowers: B. The structure and development of the fruit. Ann Bot 26:657–673

Ravikanth L, Jayas DS, White NDG, Fields PG, Sun D-W (2017) Extraction of spectral information from hyperspectral data and application of hyperspectral imaging for food and agricultural products. Food Bioprocess Technol 10(1):1–33

Rinnan Å, Berg FVD, Engelsen SB (2009) Review of the most common pre-processing techniques for near-infrared spectra. TrAC Trends Anal Chem 28:1201–1222

Robinson JC, Saúco VG (2010) Bananas and plantains. CABI

Schmutzler M, Huck CW (2016) Simultaneous detection of total antioxidant capacity and total soluble solids content by Fourier transform near-infrared (FT-NIR) spectroscopy: a quick and sensitive method for on-site analyses of apples. Food Control 66:27–37

Shenk JS, Westerhaus MO, Templeton WC (1985) Calibration transfer between near infrared reflectance spectrophotometers. Crop Sci 25:159–161

Sjöblom J, Svensson O, Josefson M, Kullberg H, Wold S (1998) An evaluation of orthogonal signal correction applied to calibration transfer of near infrared spectra. Chemom Intell Lab Syst 44:229–244

Soldado A, Fearn T, Martínez-Fernández A, De La Roza-Delgado B (2013) The transfer of NIR calibrations for undried grass silage from the laboratory to on-site instruments: comparison of two approaches. Talanta 105:8–14

Stanimirova I, Kubik A, Walczak B, Einax JW (2008) Discrimination of biofilm samples using pattern recognition techniques. Anal Bioanal Chem 390:1273–1282

Sun D-W (1997) Solar powered combined ejector vapour compression cycle for air conditioning and refrigeration. Energy Conversion and Management 38:479–491

Sun D-W (1999) Comparison and selection of EMC ERH isotherm equations for rice. Journal of Stored Products Research. Volume 35:249–264

Sun D-W, Brosnan T (1999) Extension of the vase life of cut daffodil flowers by rapid vacuum cooling. International Journal of Refrigeration-Revue Internationale Du Froid Vol 22:472–478

Sun D-W, Brosnan T (2003) Pizza quality evaluation using computer vision - Part 2 - Pizza topping analysis. Journal of Food Engineering Vol 57:91–95

Sun D-W, Zheng LY (2006) Vacuum cooling technology for the agri-food industry: Past, present and future. Journal of Food Engineering Vol 77:203–214

Tsuchikawa S (2007) A review of recent near infrared research for wood and paper. Appl Spectrosc Rev 42:43–71

Vidal M, Amigo JM (2012) Pre-processing of hyperspectral images. Essential steps before image analysis. Chemom Intell Lab Syst 117:138–148

Wang Y, Kowalski BR (1993) Temperature-compensating calibration transfer for near-infrared filter instruments. Anal Chem 65:1301–1303

Wang LJ, Sun D-W (2004) Effect of operating conditions of a vacuum cooler on cooling performance for large cooked meat joints. Journal of Food Engineering Vol 61:231–240

Wang Y, Veltkamp DJ, Kowalski BR (1991) Multivariate instrument standardization. Anal Chem 63:2750–2756

Wise BM, Gallagher NB, Bro R, Shaver JM, Windig W, Koch RS (2006) Chemometrics tutorial for PLS_Toolbox and Solo. Eigenvector Research, Inc., Wenatchee

Woodcock T, Fagan CC, O'Donnell CP, Downey G (2008) Application of near and mid-infrared spectroscopy to determine cheese quality and authenticity. Food Bioprocess Technol 1:117–129

Woody NA, Feudale RN, Myles AJ, Brown SD (2004) Transfer of multivariate calibrations between four near-infrared spectrometers using orthogonal signal correction. Anal Chem 76:2595–2600

Wu D, Sun D-W (2013) Advanced applications of hyperspectral imaging technology for food quality and safety analysis and assessment: A review - Part II: Applications. Innovative Food Science & Emerging Technologies 19:15–28

Xie A, Sun D-W, Xu Z, Zhu Z (2015) Rapid detection of frozen pork quality without thawing by Vis-NIR hyperspectral imaging technique. Talanta 139:208–215

Xie A, Sun D-W, Zhu Z, Pu H (2016) Nondestructive Measurements of Freezing Parameters of Frozen Porcine Meat by NIR Hyperspectral Imaging. Food and Bioprocess Technology 9:1444–1454

Xiong Z, Sun D-W, Pu H, Xie A, Han Z, Luo M (2015) Non-destructive prediction of thiobarbituric acid reactive substances (TSARS) value for freshness evaluation of chicken meat using hyperspectral imaging. Food Chemistry 179:175–181

Xu J-L, Sun D-W (2017) Identification of freezer burn on frozen salmon surface using hyperspectral imaging and computer vision combined with machine learning algorithm. International Journal of Refrigeration-Revue Internationale Du Froid 74:151–164

Yang Q, Da-Wen S, Weiwei C (2017) Development of simplified models for nondestructive hyperspectral imaging monitoring of TVB-N contents in cured meat during drying process. Journal of food engineering 192:53–60

Zamora-Rojas E, Pérez-Marín D, De Pedro-Sanz E, Guerrero-Ginel JE, Garrido-Varo A (2012) Handheld NIRS analysis for routine meat quality control: database transfer from at-line instruments. Chemom Intell Lab Syst 114:30–35

Zheng LY, Sun D-W (2004) Vacuum cooling for the food industry - a review of recent research advances. Trends In Food Science & Technology Vol 15:555–568